Vector magnetization depth profile of a Laves-phase exchange-coupled superlattice obtained using a combined approach of micromagnetic simulation and neutron reflectometry

M. R. Fitzsimmons,[1] S. Park,[1] K. Dumesnil,[2,3] C. Dufour,[3] R. Pynn,[1] J. A. Borchers,[4] J. J. Rhyne,[1] and Ph. Mangin[5]
[1]*Los Alamos National Laboratory, Los Alamos, New Mexico 87545, USA*
[2]*Stanford Synchrotron Radiation Laboratory, Stanford Linear Accelerator Center, 2575 Sand Hill Road, Menlo Park, California 94025, USA*
[3]*Laboratoire de Physique des Materiaux, Universite H. Poincare Nancy I, Boîte Postale 239, 54506 Vandoeuvre les Nancy Cedex, France*
[4]*National Institute of Standards and Technology, Gaithersburg, Maryland 20899, USA*
[5]*Laboratoire Léon Brillouin (UMR 12 CNRS/CEA) CEA-Saclay 91191 Gif sur Yvette, France*
(Received 12 July 2005; revised manuscript received 26 January 2006; published 13 April 2006)

Owing to the coexistence of ferromagnetic and antiferromagnetic exchange coupling in an exchange-coupled Laves-phase superlattice composed of $DyFe_2$ and YFe_2 layers, the field dependence of the magnetization depth profile is complex. Using an approach that combines micromagnetic simulation and analysis of neutron scattering data, we have obtained the depth dependence of magnetization across the $DyFe_2/YFe_2$ interfaces. We find that the exchange interaction across the interface is reduced compared to the exchange interaction of the constituent layers, thereby compromising the ability of this system to resist magnetization reversal in large applied fields.

DOI: 10.1103/PhysRevB.73.134413 PACS number(s): 75.70.Ak, 75.70.Cn, 61.12.−q

I. INTRODUCTION

Exchange-coupled magnets[1,2] or "spring" magnets are heterostructures that consist of hard and soft ferromagnetic phases. The hard ferromagnetic phase tends to resist magnetization reversal in high fields owing to its high anisotropy, while the soft phase possesses large magnetization. To the extent the two phases are exchange-coupled, the magnetization of the composite material may be both large and difficult to reverse.[3–8] Materials with such characteristics are attractive for applications requiring hard magnets, e.g., electric motors and magnetic force microscopy.[9]

Mixtures of hard and soft magnetic Laves-phase materials, of which $DyFe_2$ and YFe_2 are examples, can be grown as layered systems (superlattices) that exhibit springlike magnetic properties. $DyFe_2$ is the hard component, and YFe_2 is the soft component. A distinguishing feature of the $DyFe_2/YFe_2$ system is that each component can be grown as a single crystal,[10,11] whereas most other exchange spring systems consist of either textured polycrystalline[12,13] or amorphous materials,[14] or as mixtures of randomly oriented hard magnetic grains embedded in a soft magnetic matrix.[15–17] In contrast to conventional exchange spring systems in which the magnetizations of the hard and soft phases are parallel at remanence, the situation for Laves-phase magnetic composites is complicated by the coexistence of ferromagnetic exchange coupling among Fe moments and antiferromagnetic exchange coupling between Fe and rare-earth (RE) moments (in particular Dy). The low field magnetic structure is one with the net magnetizations of adjacent $DyFe_2$ and YFe_2 layers *antiparallel* at all temperatures (Fig. 1). Because the low field structure is well understood, and the material is single crystalline, the Laves-phase $DyFe_2/YFe_2$ superlattice enables studies of the influence of exchange and anisotropy on magnetization reversal in materials dominated by exchange coupling across interfaces.

The detailed magnetization reversal process of the superlattice depends upon a sensitive interplay between the magnetizations of the competing components (controlled by the thicknesses of the $DyFe_2$ or YFe_2 layers), the temperature dependencies of exchange coupling and anisotropy, and field strength. For systems with net magnetization dominated by the $DyFe_2$ (hard) component, the reversal process begins with the reversal of the YFe_2 (soft) magnetization as the applied field is reduced and reversed, eventually culminating in reversal of the hard magnetization for large enough fields. However, for samples with net magnetization dominated by the soft YFe_2 phase (the case of present interest), magnetization reversal exhibits unexpected behavior. For example, magnetometry data [Fig. 1(b)] show two types of ferromagnetic hysteresis consisting of small loops at the extremes of applied field and a large loop centered near zero applied field. X-ray magnetic circular dichroism[18] (XMCD) studies designed to measure the field dependence of the Dy and Y moments[19] separately showed that the smaller loops are due to reversal of the Dy moment, while the larger loop is due to reversal of the Y moment.[8,20,21] For samples in a field of $\mu_0 H \sim 7$ T at 200 or 300 K with 3 nm thick $DyFe_2$ layers, the net Dy moment is nearly zero along the applied field direction, while the net Y moment is mostly saturated.[22] This result suggests that one or more of the following scenarios occur at high fields: (1) The net Dy moment is rotated $\sim 90°$ from the large applied field. (2) Magnetic domains are formed such that the net Dy moment is zero. (3) The net Dy moment in $DyFe_2$ layer is aligned in a single domain with the net Dy moment of one $DyFe_2$ layer opposite to that of the neighboring $DyFe_2$ layers.

Since probes like XMCD or magnetometry measure the *net* magnetic response of the system, these probes cannot distinguish among the three reversal scenarios. However, each scenario yields a unique neutron scattering signature.[23]

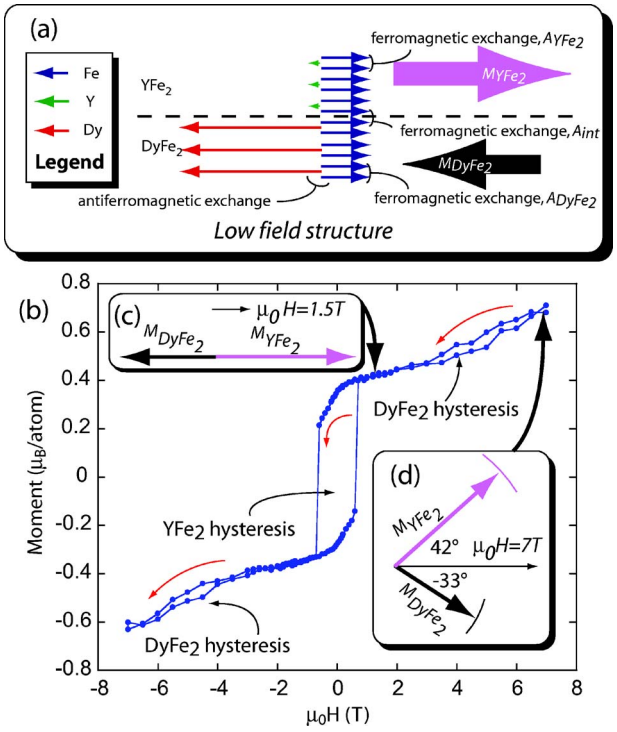

FIG. 1. (Color online) (a) Diagram (side view) of the low field (unfrustrated) configuration of Dy, Y, and Fe moments in $DyFe_2$ and YFe_2 layers. The lengths of the arrows represent the relative magnitudes of the moments. Right: The net magnetizations of the YFe_2 (purple) and $DyFe_2$ (black). The sizes of the arrows represent the relative magnitude of the net magnetizations. (b) The ferromagnetic hysteresis loop of the sample obtained from magnetometry. Locations of $DyFe_2$ and YFe_2 hysteresis as observed with XMCD are shown. (c) Schematic diagram (top view) of the low field magnetic structure. (d) Schematic diagram (top view) showing the high field structure obtained from neutron scattering (discussed in the text). The arcs indicate the confidence with which the direction of the magnetization was determined.

For example, the signatures corresponding to the three scenarios described previously are, respectively, (1) spin-flip (SF) of a polarized neutron beam, (2) off-specular diffuse scattering, and (3) 1/2-order Bragg reflections in the neutron reflectivity. In order to determine which magnetization reversal scenario is realized, we used polarized neutron reflectometry[24] to measure the depth profile of the in-plane vector magnetization of a $[(3\ \text{nm})DyFe_2/(12\ \text{nm})YFe_2]_{22}$ Laves-phase superlattice at 250 K as a function of field. To model the neutron reflectivity data, the magnetic structure is parametrized in terms of the exchange, anisotropy, and saturation magnetization, and a micromagnetic simulation is performed to obtain the spin structure. Thus, the resultant spin structures not only yield the best fit to the neutron data, they also represent minimum energy magnetic configurations.

II. SAMPLE PREPARATION AND CHARACTERIZATION

The Laves-phase superlattice was prepared by molecular beam epitaxy in a chamber with a base pressure of 4×10^{-11} Torr. A $(11\bar{2}0)$ sapphire substrate was heated to 800 °C for several hours; then allowed to cool to 700 °C prior to deposition of a 50 nm thick layer of (110) Nb buffer layer. A 1.5 nm thick Fe layer was deposited onto the Nb, and both were allowed to interdiffuse to produce a layer whose surface structure was suitable for epitaxial deposition of 22 bilayers consisting of ~3 nm thick $DyFe_2$ and 12 nm thick YFe_2. Finally, the sample was capped with 30 nm of Nb, which serves to protect the $DyFe_2/YFe_2$ bilayers from oxidation. The deposition rate was ~0.01 nm/s. The single crystalline quality of the $DyFe_2/YFe_2$ bilayers was verified with reflection high energy electron diffraction and transmission electron microscopy. The in-plane epitaxial relationships are: $[001]\text{RE-Fe}_2\|[001]\text{Nb}$ and $[1\bar{1}0]\text{RE-Fe}_2\|[1\bar{1}0]\text{Nb}$. The thicknesses of the $DyFe_2$ and YFe_2 layers were determined to be 2.8 ± 0.7 nm and 11.8 ± 1.2 nm, respectively, by x-ray reflectometry using Cu-K_α radiation, and the structural roughness of the $DyFe_2/YFe_2$ interface was determined to be 1.1 ± 0.2 nm. A comparison of the off-specular x-ray reflectivity to the specular x-ray reflectivity indicates that the roughnesses of the two interfaces were strongly correlated.[25]

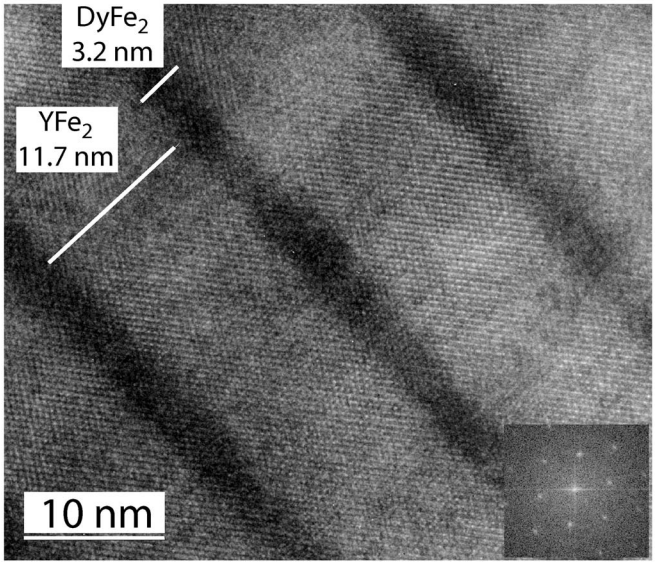

FIG. 2. Cross-sectional transmission electron micrograph of a $DyFe_2/YFe_2$ superlattice prepared in the same manner as that of the sample studied with neutron scattering.

Cross-sectional transmission electron micrographs (Fig. 2) of similarly prepared samples show sharp interfaces over lateral length scales of tens of nanometers; however, over longer lateral length scales, the interfaces zigzag by a couple nanometers in the direction along the surface normal. We conclude that the interfaces are chemically sharp locally but rough (stepped) globally, and the correlated roughness detected by the x-ray reflectometry experiment is a measure of the global roughness.

Magnetometry data taken with a superconducting quantum interference device are shown in Fig. 1(b) for a similarly prepared sample.

III. NEUTRON SCATTERING EXPERIMENT

Polarized neutron reflectometry involves reflection of a spin-polarized neutron beam from a flat sample onto a polar-

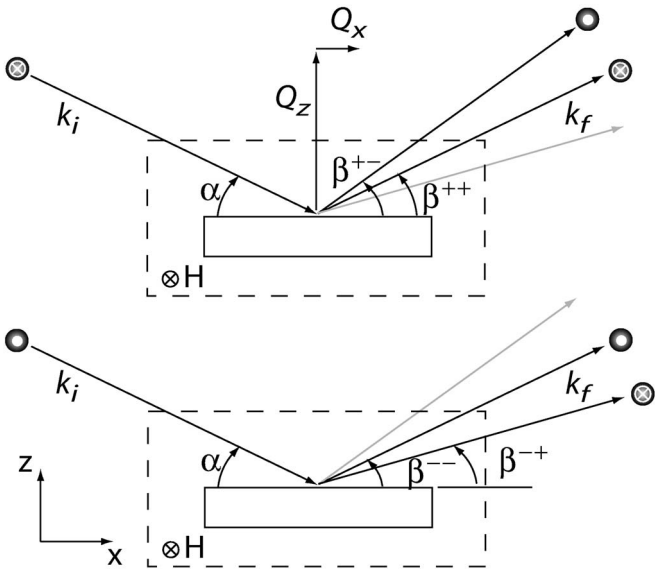

FIG. 3. Diagram showing reflection of a spin-up (upper panel) or spin-down (lower panel) incident neutron beam from a sample in a magnetic field (directed along the y axis). The angle of incidence is α, and the angle of reflection β for the associated incident and reflected neutron spin (+ denotes spin parallel to the applied field).

ization analyzer[26,27] (Fig. 3) and typically consists of four measurements: two non-spin-flip (NSF) and two spin-flip (SF) reflectivities. The NSF reflectivities correspond to the intensities for either spin-up (R^{++}) or spin-down (R^{--}) neutrons incident onto and reflected from the sample with unaltered polarization. The difference between the NSF reflectivities is related to the projection of the sample magnetization $\vec{M}(z)$ onto the direction of the applied field $\vec{H}$, i.e., $M_{\parallel}(z)$ along the y direction in Fig. 3. On the other hand, the component of $\vec{M}(z)$ that lies in the sample plane and perpendicular to $\vec{H}$, i.e., $M_{\perp}(z)$ along the x direction in Fig. 3 changes the neutron beam polarization upon reflection and produces so-called spin-flip (SF) reflectivity. SF reflectivity is related to $\langle M_{\perp}^2(z)\rangle$, where $\langle\cdots\rangle$ denotes the average taken over all domains that scatter coherently.

For our experiment, the magnetic field was applied in the sample plane and is coincident with the polarization direction of the incident neutron beam (Fig. 3). The difference between the outgoing ($\vec{k}_f$) and incoming ($\vec{k}_i$) wave vectors is the wave vector transfer $\vec{Q}$, which is nominally perpendicular to the sample surface. Prior to taking the neutron scattering measurements, the sample was cooled to 250 K in zero field, and then a magnetic field of $\mu_0 H=7$ T was applied in the sample plane at 30° from $[1\bar{1}0]$ $DyFe_2/YFe_2$. Next, the sample was rotated about its surface normal [110] $DyFe_2/YFe_2$ in the field, such that after rotation, the field was applied along $[1\bar{1}0]$ $DyFe_2/YFe_2$ during the neutron scattering experiment.[28]

Preserving neutron beam polarization in an 11 T *cryomagnet*

In order to preserve the polarization of the neutron beam as it passed through our 11 T superconducting split-pair

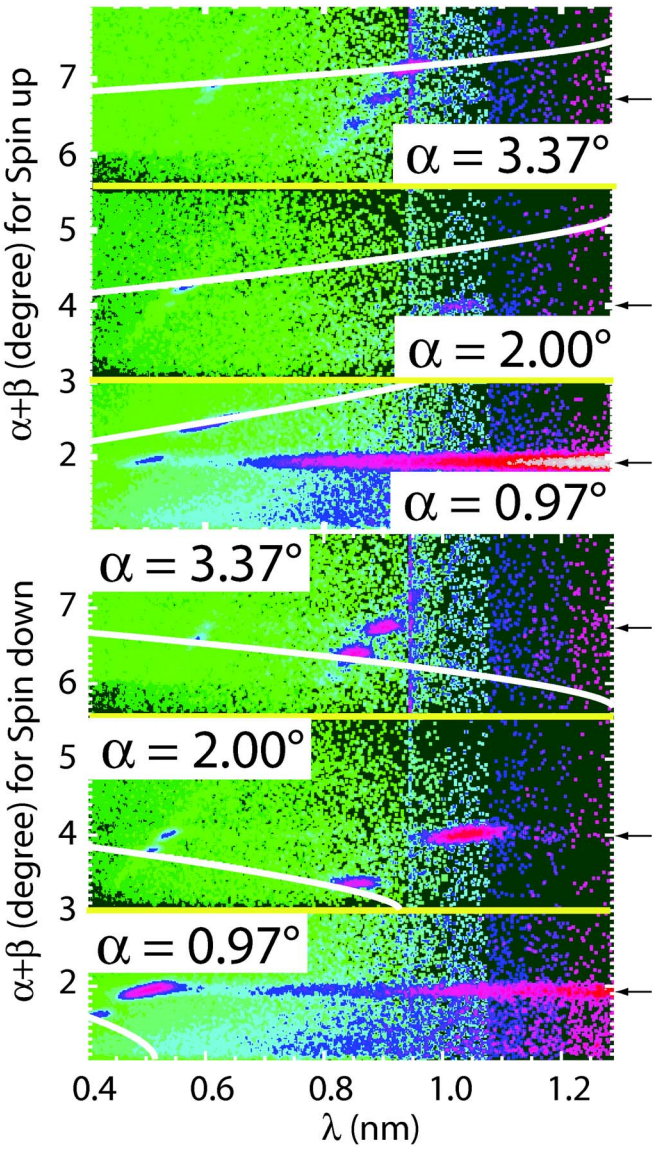

FIG. 4. (Color online) Sample reflectivity plotted vs wavelength λ, and scattering angle $\alpha+\beta$, for incident beam polarization of spin up (upper panel) and spin down (lower panel) for $\mu_0 H=7$ T. NSF specular reflectivity appears in regions centered about $\alpha+\beta=2\alpha$ (arrows). The off-specular peaks near the Bragg reflections correspond to SF reflectivity: + − (upper panel) or − + (lower panel). White curves correspond to the angular displacements of the SF reflectivity as a function of λ for $\mu_0 H=7$ T. The data shown in this figure were recorded without polarization analysis.

magnet, whose field axis is in the vertical plane (corresponding to the $+y$ direction into Fig. 3), we applied a relatively small (120 Oe) horizontal (axial) field into regions of the superconducting magnet (~20 cm from the sample) where the polarity of the field generated by the superconducting magnet switched directions (i.e., from up to down). The field was applied with permanent magnets that were securely placed in close proximity to the superconducting magnet (~0.5 cm from the cryostat's surface). The added horizontal field enables the neutron spin to follow the change of magnetic field direction adiabatically, thus preserving the polarization of the neutron beam (verified using a polarization

analyzer before the detector) as the neutrons enter and exit the superconducting magnet.[29]

IV. RESULTS

The intensity and scattering angle $\alpha+\beta$ of the neutron beam was measured with a linear position-sensitive detector as a function of three angles of incidence $\alpha=0.97$, 2.00, and 3.37°. Neutron wavelength was measured using time-of-flight techniques.[30] Measurements for $\mu_0 H=7$ T using spin-up (upper panel) and spin-down (lower panel) incident neutron beam polarizations are shown in Fig. 4. The specular reflectivity corresponds to the position in the image where $\alpha+\beta=2\alpha$. Peaks of intensity at the specular position (to the left of the arrows shown in Fig. 4) are Bragg reflections related to the periodic spacing of the $DyFe_2$ and YFe_2 layers in the superlattice. We inserted a polarization analyzer after the sample and determined that the specular reflectivity was purely non-spin-flip scattering (corrections were applied for the polarization and flipper efficiencies per Ref. 25). For the case of incident spin-up polarization (upper panel), the specular reflectivity corresponds to R^{++}. For the case of incident spin-down polarization (lower panel), the specular reflectivity corresponds to R^{--}. On the other hand, peaks of intensity that lie on the white curves above the specular reflectivity in the upper panel were purely R^{+-}, i.e., the neutron spin changed from up to down (also determined using the polarization analyzer after it was repositioned to intercept the off-specular scattering). For the case of incident spin-down polarization, the peaks of intensity that lie on the white curves below the specular reflectivity in the lower panel were purely R^{-+}.

In addition to collecting extensive measurements of the sample reflectivity at $\mu_0 H=7$ and 1.5 T, we also collected data for $\alpha\sim 2°$ at $\mu_0 H=6$, 5, and 4 T as the field was reduced from $\mu_0 H=7$ to 1.5 T. The peaks above and below the specular reflectivity shifted towards the specular reflectivity and became less intense as 5 T was approached. For $\mu_0 H<5$ T, no off-specular peaks were observed. Further, significant diffuse scattering and/or $\frac{1}{2}$-order Bragg reflections were not observed for any field at 250 K.

Influence of high magnetic fields on spin-flip scattering and neutron beam deflection

It is tempting to attribute the asymmetry in the intensities of Bragg peaks occurring in R^{+-} and R^{-+} corresponding to angles above and below the specular reflectivity, respectively, to a spiral rotation of the sample magnetization as a function of depth. Indeed, the chirality of a spiral magnetization across an Fe/La multilayer sample was inferred from an asymmetry in R^{+-} and R^{-+} for the case when $\vec{Q}$ and the polarization axis of the neutron beam were collinear.[31,32] However, in our experiment, $\vec{Q}$ is perpendicular to the polarization axis of the neutron beam—a geometry that is insensitive to the chirality of a spiral structure. Rather, the constraints of conservation of neutron energy and equality of the in-plane components of $\vec{k}_i$ and $\vec{k}_f$ across the interface require a change of angle upon reflection of a neutron when the polarization of the neutron beam flips.[33,34]

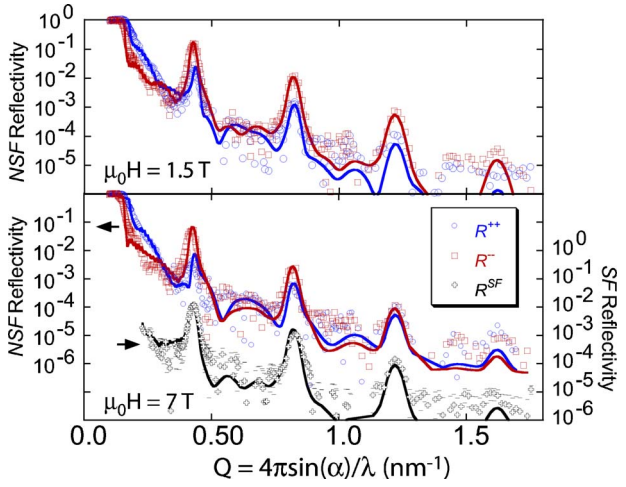

FIG. 5. (Color online) The measured (symbols) specular reflectivity of the $DyFe_2/YFe_2$ superlattice for the different neutron beam polarizations and (upper) for $\mu_0 H=1.5$ T and (lower) $\mu_0 H=7$ T. The solid curves are the reflectivities calculated from models whose vector magnetization depth profiles are shown in Fig. 6.

The relation for the reflection angle of a spin-flipped neutron in terms of the angle of incidence (in radians), field (in kOe) and wavelength λ (in Å), $\beta^2=\alpha^2\pm 1.47\times 10^{-7} H\lambda^2$, was derived in Refs. 33 and 34, where the $+(-)$ sign is used to calculate $R^{+-}(R^{-+})$. Contours given by this relation are shown as the white curves in Fig. 4 and coincide with peaks of off-specular scattering. The coincidence of the intensity peaks with λ, and the expected change of sign in polarization suggest that these peaks are the spin-flip component of the Bragg (specular) reflections that are displaced from the specular reflectivity due to the change of Zeeman energy ($\sim$0.44 μeV) of the neutron. Finally, the positions of the off-specular peaks observed at 6 T coincided with contours calculated using the smaller field (not shown), adding further weight to our explanation for the shift of these peaks away from the specular ridge. We note that testing the dependence of β on λ and H by varying λ is a better approach than varying H, since a change of H can alter the magnetic structure of the system.

In large fields, we were able to discern SF from NSF reflectivity without a polarization analyzer because specularly reflected neutrons that are spin-flipped are spatially separated from non-spin-flip neutrons by the Zeeman effect.[35] To obtain R^{SF}, we calculated the average of the intensities along contours above the specular reflectivity (giving R^{+-}) with those below the specular reflectivity (giving R^{-+}) corresponding to the same Q. The specular polarized neutron reflectivities of the sample for $\mu_0 H=7$ and 1.5 T are shown in Fig. 5, after removal of instrumental background and correction for polarization efficiencies (incident neutron beam polarization $\sim$91%) per Ref. 25.

V. DISCUSSION

There are two noteworthy features in the data (Fig. 5). First, the intensities of the NSF Bragg reflections change

TABLE I. Magnetization, anisotropy and exchange constants for the $DyFe_2/YFe_2$ superlattice

	$DyFe_2$	YFe_2	interface
M (emu/cm^3)	340 ± 90	550 ± 70	—
K (erg/cm^3)	$(1.2\pm0.7)\times10^8$	$1.3\times10^6\begin{cases}+5.7\times10^6\\-1.3\times10^6\end{cases}$	—
A (erg/cm)	$3.4\times10^{-6}\begin{cases}+4.5\times10^{-6}\\-3.1\times10^{-6}\end{cases}$	$(2.8\pm2.0)\times10^{-5}$	$(2.7\pm0.7)\times10^{-7}$

with field. Specifically, Bragg reflections for R^{--} are always more intense than those for R^{++} when $\mu_0 H=1.5$ T. However, in higher fields, the intensities of Bragg reflections for R^{++} become increasingly larger with Q, compared to those for R^{--}. Since the specular reflectivity is related to the depth dependence of the scattering medium, the redistribution of Bragg intensities with Q and H imply that the magnetic structure of the sample projected along H is not uniform across the $DyFe_2/YFe_2$ bilayers when H is large.

The second noteworthy feature is the lack of SF reflectivity for $\mu_0 H=1.5$ T and strong SF reflectivity for $\mu_0 H=7$ T. The lack of SF reflectivity at 1.5 T, which was verified by using the polarization analyzer (since the small field will no longer suffice to separate NSF and SF reflectivity in scattering angle), suggests that $\langle M_\perp^2(z)\rangle$ is near zero, i.e., no rotation of the vector magnetization in the sample plane away from the applied field was detected. Consequently, the Fe moments are parallel to the applied field, and ferromagnetic exchange between the Fe moments in the $DyFe_2$ and YFe_2 layers is not frustrated (in low field).

For $\mu_0 H \geqslant 6$ T, SF reflectivity is observed indicating that larger applied fields cause rotation of some component of the $DyFe_2/YFe_2$ bilayer magnetization away from the applied field. The influence of field on rotation of the sample magnetization suggests that the Zeeman energy cost in having a portion of the $DyFe_2/YFe_2$ bilayer net magnetization antiparallel to the applied field becomes too great. Consequently, the $DyFe_2$ magnetization rotates, and domain walls form in the superlattice.

Micromagnetic simulation and neutron scattering analysis—a combined approach

Quantitative information about the spatial variation of the vector magnetization across the $DyFe_2/YFe_2$ superlattice was obtained by combining micromagnetic simulation with analysis of the Q dependence of the neutron reflectivity—the latter calculated using the dynamical formalism of Parratt.[36] The vector magnetization depth profile was represented by a one-dimensional chain of N magnetic moments with a spacing corresponding to the nearest neighbor spacing of Fe moments parallel to the (110) plane in $DyFe_2$ or YFe_2 (0.1727 nm), subject to the constraint that the net magnetization of YFe_2 ($DyFe_2$) was parallel (antiparallel) to the Fe moment. The orientation ϕ_i of the ith Fe moment relative to the applied field H was obtained by minimizing the total magnetic energy, E [Eq. (1)]—the sum of the exchange, anisotropy, and Zeeman energies,[37,38]

$$E=-\sum_{i=1}^{N-1}\frac{A_{i,i+1}}{d_{i,i+1}^2}\cos(\phi_{i+1}-\phi_i)+\sum_{i=1}^{N}K_i\sin^2(\phi_i+\varepsilon)-H\sum_{i=1}^{N}M_i\cos(\phi_i+\theta_i). \quad (1)$$

A $DyFe_2/YFe_2$ bilayer was modeled by a chain of 15 moments representing the ~3 nm thick $DyFe_2$ layer followed by a chain of 75 moments representing the ~12 nm thick YFe_2 layer. The superlattice was represented by repeating the bilayer block 22 times. The energy was computed using Eq. (1) with the exchange A_{int} across the $DyFe_2/YFe_2$ interface, the exchanges A_{DyFe2} and A_{YFe2}, the anisotropies K_{DyFe2} and K_{YFe2}, and magnetizations M_{DyFe2} and M_{YFe2} for the $DyFe_2$ and YFe_2 layers, respectively. Since the field was applied along the easy axis of the superlattice, $\varepsilon=0$. For Fe moments in YFe_2, $\theta=0$ (since the magnetization of YFe_2 was parallel to the Fe moment), and for Fe moments in $DyFe_2$, $\theta=\pi$ (since the magnetization of the $DyFe_2$ layer was antiparallel to the Fe moment). The energy was minimized by perturbing ϕ_i for randomly selected moments subject to the condition that $dE/d\phi_i=0$, until the fractional change of energy was less than one part in 10^7.

For each field, the magnetic structure of the superlattice was obtained from an iterative process that involved: (1) selecting values for A, K, and M, (2) determining ϕ_i for all i that minimized E, (3) calculating the magnetic vector contribution to the neutron scattering length density profile from ϕ_i,[23] (4) calculating the neutron reflectivities using the scattering length density profile,[23] (5) computing a goodness-of-fit metric χ^2 between the calculated and observed reflectivities,[39] and (6) determining perturbations to the parameters A, K, and M that reduced χ^2 using the Powell optimization procedure.[40] Steps 2 through 6 were repeated until χ^2 was minimized yielding optimum values of A, K, and M.[41] The neutron scattering length density profile also contains information about the depth dependence of the chemical structure, e.g., layer widths[42] and interface roughness, which was obtained from x-ray reflectometry. Attenuation of the reflectivity due to chemical and magnetic roughness was treated using a damped exponential [$=\exp(-Q^2\sigma^2)$].

Owing to the strong exchange coupling and anisotropy intrinsic to $DyFe_2$ and YFe_2, the magnetic structure is unlikely to be affected by low magnetic fields—the structure is much like that shown in Figs. 1(a) and 1(c). Therefore, we used the data obtained in low field $\mu_0 H=1.5$ T to determine

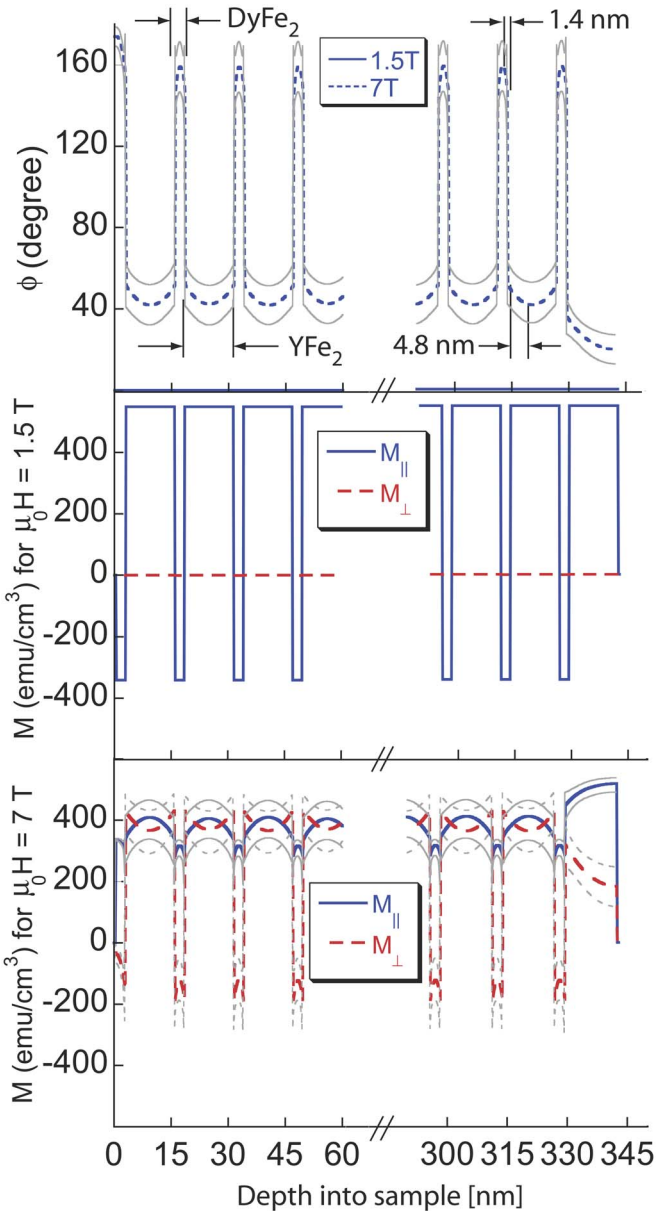

FIG. 6. (Color online) Upper: The depth profiles showing the directions of the Fe moments ϕ in the superlattice with respect to the applied field. The gray curves indicate the range over which ϕ changes within the limits of the parameters given in Table I from which the magnetic structure is derived. Middle: The components of the net sample magnetization parallel $M_{\|}(z)$ and perpendicular $M_{\perp}(z)$ for $\mu_0 H = 1.5$ T. Lower: The components $M_{\|}(z)$ and $M_{\perp}(z)$ for $\mu_0 H = 7$ T. The gray curves represent the range over which $M_{\|}(z)$ and $M_{\perp}(z)$ (for $\mu_0 H = 7$ T) change within the limits given in Table I.

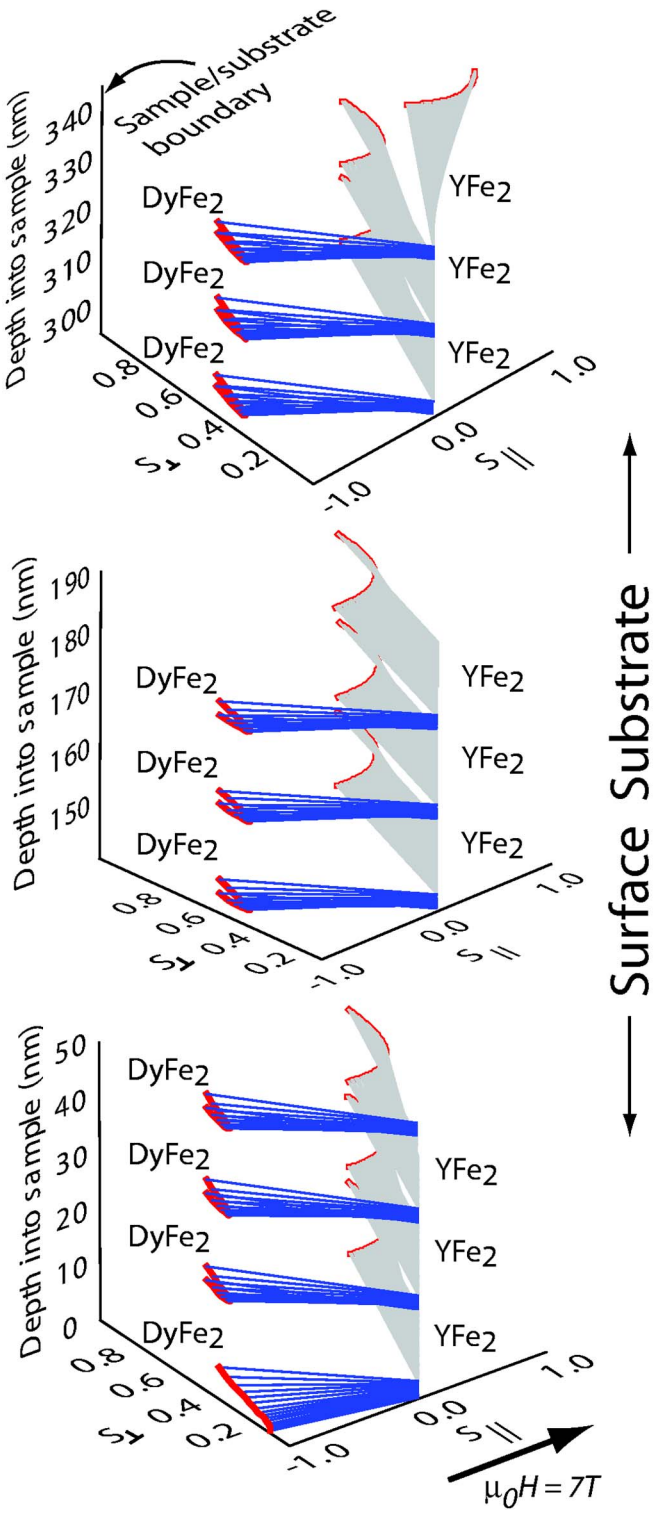

FIG. 7. (Color online) Three-dimensional rendering of the Fe moment directions near the top and bottom of the sample obtained from the information in Fig. 6. The $DyFe_2$ layers are colored blue (dark gray).

the values of M_{DyFe2} and M_{YFe2}. Since the field, magnetizations, and Fe moments are all parallel (or antiparallel), the contribution to the magnetic energy from anisotropy is zero; therefore, the values of K_{DyFe2} and K_{YFe2} do not play a role in determining the magnetic structure of the superlattice in low field. The exchange across the interface A_{int} is important in determining the low field magnetic structure only to the extent that the interface exchange is large enough to force the magnetization of the $DyFe_2$ layer to be opposite the low applied field, otherwise the low field magnetic structure is mostly insensitive to the exchange. For analysis of the low field data, we used exchanges in the range

$0.3-2\times10^{-6}$ erg/cm which are observed for bulk Fe.[43] (The analysis of the high field data is more sensitive to the values of A_{int}, A_{DyFe2}, and A_{YFe2}. Once these values were obtained, we checked whether they influenced the low field analysis, and they did not.) The values of $M_{DyFe2}=340\pm90$ emu/cm^3 and $M_{YFe2}=550\pm70$ emu/cm^3 (Table I), yielded the best fitting structure shown in Fig. 6 whose reflectivity is shown as the solid curve in Fig. 5 (upper panel).[44] Our values of M_{DyFe2} and M_{YFe2} are reasonable in comparison to values that range from 263 to 868 emu/cm^3 for $DyFe_2$ and 659 to 857 emu/cm^3 for YFe_2 derived from $\mu_{Dy}=6$ to 7.6 μ_B and μ_{Fe} of 1.77 μ_B (YFe_2 bulk), 1.5 μ_B ($DyFe_2$ bulk) and 2.3 μ_B (YFe_2 or $DyFe_2$ film) reported in Ref. 7 for 300 K. In addition to the two fitted magnetic parameters, the nuclear scattering lengths of $DyFe_2$ and YFe_2 were also optimized (since there is no relation between x-ray and neutron scattering lengths). The interface roughness σ was also optimized, but constrained to the range of 1.1 ± 0.2 nm obtained with x-ray reflectometry.[45] The goodness-of-fit between the reflectivity data and fitted curve for the low field measurement was $\chi^2_\nu=29$ for $\nu=575$ (the number of degrees of freedom).[46]

Of paramount interest are the values of K and A for the constituent components and the interface exchange A_{int}. These values can be obtained by examining the response of the magnetic structure to fields of several T (for our system), so the analysis described in the previous paragraph was performed for the data taken in high field $\mu_0H=7$ T. However, in this instance the nuclear scattering length densities for $DyFe_2$ and YFe_2 and their magnetizations, M_{DyFe2} and M_{YFe2} were fixed to those obtained from analysis of the low field data. Thus, the magnetic structure in high field was obtained by varying only the values of K_{DyFe2}, K_{YFe2}, A_{DyFe2}, A_{YFe2}, and A_{int}. The optimal values of these parameters (see Table I) yielded the magnetic structure shown in Figs. 6 and 7, whose reflectivity is shown by the solid curves in Fig. 5 (lower panel). The goodness-of-fit between the reflectivity data and fitted curves for the high field measurement was $\chi^2_\nu=33$ for $\nu=778$. Rotation of the Fe moments extends throughout the $DyFe_2$ layer, and approximately 4.8 nm into the YFe_2 layer (see Fig. 6, upper panel, and Fig. 7). Considering only the interior layers, the Fe moments rotate over a range of 105° from a peak value of $147\pm12°$ in the $DyFe_2$ layer to $42\pm10°$ in the YFe_2 layer.

Not surprisingly, the magnetizations of the two outermost magnetic layers (one is $DyFe_2$ and the other is YFe_2) are mostly parallel to the large applied field (see Fig. 6, lower panel, where $M_\perp\rightarrow0$ at the sample boundaries), because these layers lack symmetric restoring forces that are characteristic of interior layers. The magnetizations of the interior $DyFe_2$ and YFe_2 layers point $-33\pm12°$ and $42\pm10°$, respectively, from the applied field [a schematic example of two such layers is shown in Fig. 1(d)].

The qualitative picture of the magnetization reversal process obtained from our quantitative analysis is as follows: First, in a low applied field $\mu_0H=1.5$ T, the $DyFe_2$ magnetization is opposite to the field, while that of the YFe_2 is parallel to the field [see Fig. 1(c)]. As the field is increased the $DyFe_2$ magnetization rotates towards the field. For $\mu_0H=7$ T the $DyFe_2$ magnetization has rotated 147° about the sample's surface normal [shown as a counter-clockwise rotation in Fig. 1(c)] to be at an angle of −33° with respect to the applied field. In addition, the YFe_2 magnetization has rotated in the same direction but by a smaller amount (the YFe_2 magnetization having started at 0° relative to the $\mu_0H=1.5$ T field) to be at an angle of 42° to the applied field. The resulting configuration in high field is one with the components of the $DyFe_2$ and YFe_2 magnetizations perpendicular to the applied field having an antiparallel arrangement. Such a spin-flop configuration is a low energy configuration.[47]

The picture of a magnetization reversal process that involves rotation of both $DyFe_2$ and YFe_2 magnetizations obtained from neutron scattering is somewhat different than that inferred from XMCD from which only the net Dy moment was observed to change when the field was increased from $\mu_0H=1.5$ to 7 T. The different pictures might stem from differences in the sample's magnetic history prior to the experiments. However, we note that the two techniques measure different quantities. When tuned to the appropriate x-ray resonance, XMCD can be made sensitive to either the Dy or Y moments, while neutron scattering is sensitive to the magnetizations of the $DyFe_2$ and YFe_2 layers. If the net magnetization of a layer is not parallel to the rare earth moment, then the two techniques will yield different (but complementary) results.

The average magnetization projected onto the $\mu_0H=7$ T field has a value of $\langle M_\parallel\rangle=379\pm47$ emu/cm^3 (obtained by computing the average of $M_\parallel(z)$ from Fig. 6), which can be compared to the magnetization obtained with magnetometry for the same field.[48] Using for the atomic volume of YFe_2 a value of $\Omega=0.398$ nm^3 in which eight YFe_2 formula units are contained,[49] we obtain $\langle M_\parallel\rangle=0.68\pm0.08$ μ_B/atom (from the neutron scattering experiment).[50] This value is in excellent agreement with that of 0.71 μ_B/atom obtained from magnetometry [Fig. 1(b)].

The optimum value for the anisotropy of the $DyFe_2$ layer is about three times larger than that for bulk $DyFe_2$ of 4.2×10^7 erg/cm^3 (Refs. 8, 51, and 52) (a difference that might be attributed to epitaxial strain in the superlattice), although our value is somewhat uncertain, and the difference may not be significant. Nevertheless, the anisotropy of the $DyFe_2$ layer is significantly greater than zero. On the other hand, the anisotropy of the YFe_2 layer was determined with much less precision, although the range of values is significantly smaller than that of $DyFe_2$. We note that for bulk materials, K_{YFe2} (1×10^6 erg/cm^3) (Refs. 8, 51, and 52) is much smaller than K_{DyFe2}.

The $DyFe_2/YFe_2$ interfacial exchange A_{int} is at the low end of the range $0.3-2\times10^{-6}$ erg/cm reported for exchange in bulk Fe (a magnetically soft material).[43,53] An important result of our analysis is that the interfacial exchange is one to two orders of magnitude smaller than the exchange found in the constituent layers. Therefore, the response of the $DyFe_2$ magnetization to large applied fields can be attributed to a balance between the *reduced exchange coupling across the* $DyFe_2/YFe_2$ *interface* and the *Zeeman energy of the magnetic components*. We note values of A_{int} somewhat larger than that reported in Table I yield magnetic structures (ob-

tained from the micromagnetic simulation) with the $DyFe_2$ magnetization opposite to the large applied field, while somewhat smaller values yield structures with both $DyFe_2$ and YFe_2 magnetizations aligned parallel to the large field. Neither configuration is observed with XMCD or neutron scattering for $\mu_0 H = 7$ T in the temperature range of 200 to 300 K.

VI. CONCLUSIONS

In summary, we have used polarized neutron reflectometry to measure the influence of low ($\mu_0 H = 1.5$ T) and high ($\mu_0 H = 7$ T) magnetic fields on the magnetization depth profile of a $DyFe_2/YFe_2$ Laves-phase superlattice. In low fields, we find an antiparallel arrangement of $DyFe_2$ and YFe_2 magnetizations (a result consistent with the directions of Dy and Y moments obtained with XMCD), and the antiparallel arrangement exhibits long-range order with the $DyFe_2$ magnetization rotated 180° from the direction of the low applied field. The magnitude of the $DyFe_2$ magnetization implies that the Dy and Fe moments are antiparallel. Thus, ferromagnetic coupling of Fe moments is not frustrated in this system by low or moderate fields, since these moments are parallel throughout the superlattice.

The absence of significant diffuse scattering and 1/2-order Bragg reflections allows us to conclude that high magnetic fields do not induce formation of magnetic domains or an antiparallel arrangement of spin-flopped magnetic layers that conspire to produce no net magnetization along the applied field direction at 250 K. Rather, the $DyFe_2$ magnetization and to a lesser extent the YFe_2 magnetization primarily rotate in response to field. Specifically, the magnetization of $DyFe_2$ (except for $DyFe_2$ near the top of the sample) is rotated $-33 \pm 12°$ from the field, while the magnetization of the YFe_2 (except for YFe_2 near the bottom of the sample) deviates from the applied field by $42 \pm 10°$. The 75° separation between the $DyFe_2$ and YFe_2 magnetizations is a consequence of a 105° domain wall between the Fe moments across the $DyFe_2/YFe_2$ interface extending throughout the $DyFe_2$ layer and 4.8 nm into the YFe_2 layer.

Since the magnetic structure was obtained by combining micromagnetic simulation with analysis of the neutron scattering data, we were able to show that the response of the Fe moment depth profile and concomitant response of the $DyFe_2$ and YFe_2 layer magnetizations were due to the greatly diminished exchange coupling across the $DyFe_2/YFe_2$ interface compared to the Fe-Fe exchange coupling in either layer. The value of the interfacial exchange is similar to that of bulk Fe (a soft magnetic material). Our approach assures that the magnetic structure deduced from the neutron scattering data is also one that minimizes the magnetic energy for a given set of K, A, and M's. For our particular problem, micromagnetic simulation yielded physically realistic perturbations to the magnetic structure at both ends of the superlattice (arising from the lack of competing exchange interactions on either surface) and led to an improved fit between the observed and calculated neutron reflectivities. An additional advantage of our approach is that the fitted parameters, e.g., exchange, anisotropy, and saturation magnetization, are ones that have practical meaning.

ACKNOWLEDGMENTS

Use of the Manuel Lujan Jr. Neutron Scattering Center is gratefully appreciated. This work was supported by the Office of Basic Energy Science, U.S. Department of Energy (contract No. W-6405-Eng-36) and Laboratory Directed Research and Development program funds. We gratefully acknowledge E. Snoeck (CEMES, Toulouse, France) for providing the transmission electron micrograph and its analysis.

[1] E. F. Kneller and R. Hawig, IEEE Trans. Magn. **27**, 3588 (1991).
[2] E. E. Fullerton, J. S. Jiang, M. Grimsditch, C. H. Sowers, and S. D. Bader, Phys. Rev. B **58**, 12193 (1998).
[3] K. V. O'Donovan, J. A. Borchers, C. F. Majkrzak, O. Hellwig, and E. E. Fullerton, Phys. Rev. Lett. **88**, 067201 (2002).
[4] K. V. O'Donovan, J. A. Borchers, S. Maat, M. J. Carey, and B. A. Gurney, J. Appl. Phys. **95**, 7507 (2004).
[5] C. Dufour, K. Cherifi, G. Marchal, P. Mangin, and M. Hennion, Phys. Rev. B **47**, 14572 (1993).
[6] W. Hahn, M. Loewenhaupt, Y. Y. Huang, G. P. Felcher, and S. S. P. Parkin, Phys. Rev. B **52**, 16041 (1995).
[7] M. J. Bentall, R. A. Cowley, W. J. L. Buyers, Z. Tun, W. Lohstroh, R. C. C. Ward, M. R. Wells, J. Phys.: Condens. Matter **15**, 4301 (2003).
[8] K. Dumesnil, C. Dufour, Ph. Mangin, and A. Rogalev, Phys. Rev. B **65**, 094401 (2002).
[9] J. O. Oti, P. Rice, and S. E. Russek, J. Appl. Phys. **75**, 6881 (1994).
[10] K. Dumesnil, M. Dutheil, C. Dufour, and Ph. Mangin, Phys. Rev. B **62**, 1136 (2000).
[11] E. E. Fullerton, J. S. Jiang, and S. D. Bader, J. Magn. Magn. Mater. **200**, 392 (1999).
[12] O. Hellwig, J. B. Kortright, K. Takano, and E. E. Fullerton, Phys. Rev. B **62**, 11694 (2000).
[13] F. Radu, M. Etzkorn, R. Siebrecht, T. Schmitte, K. Westerholt, and H. Zabel, Phys. Rev. B **67**, 134409 (2003).
[14] S. Mangin, G. Marchal, and B. Barbara, Phys. Rev. Lett. **82**, 4336 (1999).
[15] R. Coehoorn, D. B. De Mooij, and C. De Waard, J. Magn. Magn. Mater. **80**, 101 (1989).
[16] L. H. Lewis, J. Kim, and K. Barmak, Physica B **327**, 190 (2003).
[17] H. Zeng, J. Li, J. P. Lu, Z. L. Wang, and S. Sun, Nature **420**, 395 (1999).
[18] J. B. Kortright, in *Modern Techniques for Characterizing Magnetic Materials*, edited by Y. Zhu (Kluwer Academic Publishers, Boston, 2005), Chap. 4, p. 159.
[19] The Y moment is understood to be that induced by its proximity to Fe in YFe_2.
[20] K. Dumesnil, C. Dufour, Ph. Mangin, M. R. Fitzsimmons, S. Park, J. J. Rhyne, A. Rogalev, and J. A. Borchers, J. Appl. Phys.

97, 10K108 (2005).
[21] K. Dumesnil, C. Dufour, Ph. Mangin, A. Rogalev, and F. Wilhelm, J. Phys.: Condens. Matter **17**, L215 (2005).
[22] For temperatures less than 300 K, the $DyFe_2$ magnetization of our sample is antiparallel to low ($\mu_0 H \sim 1$ T) applied fields.
[23] M. R. Fitzsimmons and C. F. Majkrzak, in *Modern Techniques for Characterizing Magnetic Materials*, edited by Y. Zhu (Kluwer Academic Publishers, Boston 2005), Chap. 3, p. 107.
[24] M. R. Fitzsimmons, S. D. Bader, J. A. Borchers, G. P. Felcher, J. K. Furdyna, A. Hoffmann, J. B. Kortright, Ivan K. Schuller, T. C. Schulthess, S. K. Sinha, M. F. Toney, D. Weller, and S. Wolf, J. Magn. Magn. Mater. **271**, 103 (2004).
[25] S. Park, M. R. Fitzsimmons, X. Y. Dong, B. D. Schultz, and C. J. Palmstrøm, Phys. Rev. B **70**, 104406 (2004).
[26] G. P. Felcher, R. O. Hilleke, R. K. Crawford, J. Haumann, R. Kleb, and G. Ostrowski, Rev. Sci. Instrum. **58**, 609 (1987).
[27] C. F. Majkrzak, Physica B **221**, 342 (1996).
[28] At 250 K the easy axis of $DyFe_2/YFe_2$ is believed to be close to the in-plane direction of $[1\bar{1}0]$ $DyFe_2/YFe_2$. By applying a field 30° off this axis, and then rotating the easy axis of the sample parallel to the field, we intended to promote rotation of the sample magnetization in the same sense across the sample and thus growth of a large single magnetic domain. No deliberate attempt to break the crystal symmetry was made prior to the XMCD experiments.
[29] By projecting a horizontal field component into the outer periphery of the superconducting magnet, the neutron beam polarization could be maintained while operating the magnet in so-called symmetric mode—a mode in which equal currents pass through each superconducting coil, thus enabling access to the highest possible magnetic fields.
[30] Three angles of incidence are required to measure Q from 0.1 to 1.8 nm^{-1} with neutron wavelengths ranging from 0.4 to 1.2 nm.
[31] G. P. Felcher, W. Lohstroh, H. Fritzsche, M. Münzenberg, H. Maletta, and W. Felsch, Appl. Phys. Lett. **72**, 2894 (1998).
[32] M. Blume, Phys. Rev. **130**, 1670 (1963).
[33] G. P. Felcher, S. Adenwalla, V. O. De Haan, and A. A. Van Well, Physica B **221**, 494 (1996).
[34] G. P. Felcher, S. Adenwalla, V. O. De Haan, and A. A. Van Well, Nature **377**, 409 (1995).
[35] In low fields, we were forced to use a polarization analyzer—to determine that there was no SF reflectivity.
[36] L. G. Parratt, Phys. Rev. **95**, 359 (1954).
[37] E. Goto, N. Hayashi, T. Miyashita, and K. Nakagawa, J. Appl. Phys. **36**, 2951 (1965).
[38] E. E. Fullerton, J. S. Jiang, and S. D. Bader, J. Magn. Magn. Mater. **200**, 392 (1999).
[39] W. H. Press, S. A. Teukolsky, W. T. Vetterline, and B. P. Flannery, *Numerical Recipes: The Art of Scientific Computing* (Cambridge University Press, Cambridge, England, 1986), p. 70.
[40] W. H. Press, S. A. Teukolsky, W. T. Vetterline, and B. P. Flannery, *Numerical Recipes: The Art of Scientific Computing* (Cambridge University Press, Cambridge, England, 1986), p. 294.
[41] The refinement required nearly two weeks to complete using a 1.2 GHz microprocessor.
[42] The locations of the neutron Bragg reflections indicated layer thicknesses of 2.5 and 13 nm for $DyFe_2$ and YFe_2, respectively, which were somewhat different—though acceptably similar—to those obtained from x-ray reflectometry.
[43] B. D. Cullity, *Introduction to Magnetic Materials* (Addison-Wesley Publishing Co., Reading, MA, 1972), p. 397.
[44] The error bar represents the perturbation to the parameter that yielded an increase in $\chi_\nu^2 = \chi^2/\nu$ by four (where ν is the number of observations minus the number of optimized parameters).
[45] Fitting to the low field data yielded an optimum value of $\sigma = 1.29$ nm.
[46] One expects χ_ν^2 to approach unity.[39] Our values are larger because the superlattice reflections are slightly aperiodic in Q at the level of a couple parts in 10^4. The small deviation of the superlattice reflection is a consequence of our inability to exert the required control over the location of our detector, when we use the 11 T superconducting magnet.
[47] J. S. Jiang, G. P. Felcher, A. Inomata, R. Goyette, C. Nelson, and S. D. Bader, Phys. Rev. B **61**, 9653 (2000).
[48] A magnetometer typically measures the component of a sample's magnetization along the applied field.
[49] PCPDFWIN, version 2.02, May 1999 (JCPDS-ICDD, 1999).
[50] We have used the atomic volume of YFe_2 (0.398 nm^3) instead of $DyFe_2$ (0.393 nm^3), because the sample is mostly YFe_2.
[51] V. Oderno, C. Dufour, K. Dumesnil, Ph. Bauer, Ph. Mangin, G. Marchal, L. Hennet, and G. Patrat, Europhys. Lett. **36**, 713 (1996).
[52] A. Mougin, C. Dufour, K. Dumesnil, and Ph. Mangin, Phys. Rev. B **62**, 9517 (2000).
[53] We note that the magnetic structure for an applied field $\mu_0 H = 1.5$ T is not affected whether the values of K and A used in the simulation were those shown in the table or those of the bulk material or their average for the interface.